Predicting Fault Locations based on Morphometric Features of Alluvial Fans and Basins using Artificial Neural Networks

Marzieh Mokarram (m.mokarram@shirazu.ac.ir)
Shiraz University https://orcid.org/0000-0003-4282-1950
Hamid Reza Pourghasemi
Shiraz University
John P. Tiefenbacher
Texas State University

Research Article

Keywords: Morphometric features, Alluvial fan, Fault, Erosion, Principal component analysis (PCA) method, Adaptive neural-fuzzy network (ANFIS)

Posted Date: June 16th, 2021

DOI: https://doi.org/10.21203/rs.3.rs-607932/v1

Predicting fault locations based on morphometric features of alluvial fans and basins using artificial neural networks

Marzieh Mokarram[1*] Hamid Reza Pourghasemi[2] John P. Tiefenbacher[3]

[1]Department of Range and Watershed Management, College of Agriculture and Natural Resources of Darab, Shiraz University, Iran, ORCID ID: https://orcid.org/0000-0003-4282-1950. Email: m.mokarram@shirazu.ac.ir*

[2]Department of Natural Resources and Environmental Engineering, College of Agriculture, Shiraz University, Shiraz, Iran, Email: hr.pourghasemi@shirazu.ac.ir

[3]Department of Geography, Texas State University, San Marcos, TX USA, Email: tief@txstate.edu

***[*]Corresponding author:** MarziehMokarram, Tel.: +98-917-8020115; Fax: +987153546476 Address: Darab, Shiraz university, Iran, Postal Code: 71946-84471, Email: m.mokarram@shirazu.ac.ir*

Predicting fault locations based on morphometric features of alluvial fans and basins using artificial neural networks

Abstract

The aim of this study is to investigate the morphometry of alluvial fans located in the vicinity of the Sabzevar and Sang-Sefid faults in northeastern Iran to determine their influence on erosion Principal component analysis (PCA) was used to select the most important morphometric factors affecting erosion. The data regarding the important parameters were input into adaptive neural-fuzzy networks (ANFIS) to predict erosion rates. The asymmetric factor (*Af*), hypsometric integral (Hi), and basin shape (BS) indicate that most of the sub-basins are tectonically active. The results of the PCA revealed that the most important parameters affecting erosion were A_f, P_f, L_f, R_f, V_f, P_b, A_b, LC, L_b, Dd, and the geological unit. The ANFIS method showed that among the soil erosion prediction models, the FCM hybrid model had the highest accuracy. It is concluded that morphometric features can be used to predict the erosion processes in the basin.

Keywords: Morphometric features, Alluvial fan, Fault, Erosion, Principal component analysis (PCA) method, Adaptive neural-fuzzy network (ANFIS).

Introduction

As a river flows out of a mountainous region and enters a plain with a low slope, the capacity for carrying sediment is reduced and an alluvial fan forms (Lancaster et al. 2012) (Fig. S1). Alluvial fans are prominent geomorphological features that form in several climates (Radebaugh et al. 2013). The head of the alluvial fan is located at the site of gradient change, where the stream leaves the mountainous slopes and its base or toe is where the stream exits the fan at its downstream end (Benito 2013).

The sediment of alluvial fans includes sand, gravel, silt, and clay, which increase the particle size from upstream to downstream. Deposits near the top or apex of the fan are mostly coarse-grained rock fragments

and large rubble. Sediments become increasingly fine toward the base, where they are grains of sand, gravel, marl, and clay. Alluvial fans are widespread in arid and semi-arid areas where vegetation is sparse. Some alluvial fans are good sources of aggregates that can be used in construction (Langer et al. 2004).

Alluvial fans are affected by an assortment of variables that change from location to location. Alluvial fan processes depend on five factors: lithology, basin shape, conditions in the alluvial fan environment, climate, and tectonic activity (Blair and McPherson 1994). These factors, especially climate and tectonics, affect the inlet and outlet energy (Stokes and Mather 2000; Sancho et al. 2008).

These include lithology, basin shape, conditions of the alluvial fan environment, climate, and tectonic activity. These factors, especially climate and tectonics, relate to the inlet and outlet energy. The directions of slopes, the profiles of the channels feeding the alluvial fan, unevenness or relief, flash flood risk, and sediment storage capacity are related to the morphometry of the alluvial fan. Alluvial fans have been found to be useful for studying floods may be studied (Khan et al. 2013). Climate and climate change have significant effects on the morphometry of alluvial fans, because water availability has a direct effect on weathering, sediment production, and vegetation, and climatic conditions control alluvial currents (Harvey et al. 1999).

Tectonic activity can induce changes in alluvial fans, particularly affecting their morphometry (Harvey 1987). Regardless of the permanence of tectonic activity, alluvial fans are small and short-lived (Parsons, 2009). Orographic uplift can generate new sediments that may be deposited on alluvial fans (Beaty 1963). The displacement of the right-slip faults at the alluvial fan formation causes displacement of the alluvial fans and their surface flow. The slope and morphological characteristics of the alluvial fan surface were also somewhat controlled by tectonics. The morphological characteristics of the fans are evidence of tectonic activity (Bull 2007).

It is very difficult to study alluvial fans in forested areas and deserts. It is also difficult and time consuming to study alluvial fans over large regions (Foster and Beaumont 1992). Using GIS, algorithms, and DEMs, alluvial fans can be more easily observed and analyzed in watersheds and they can be easily

distinguished from upstream basins (Lagmay et al. 2013). The extraction of geological information from topographic data sets is very important in land studies, but these data can be more easily gathered using a DEM (Fleming et al. 2010). DEMs have been used in studies of volcanoes, faults, slope stability, and landslides. By measuring factors such as elevation and elevation with DEMs, geomorphological features such as cones, volcanoes, fans, and slopes can be analyzed (Eisank et al. 2014). Investigation of the morphometric characteristics of alluvial fans enables the prediction of superficial activities, such as erosion and deposition, as well as internal activities such as tectonics (Roberts and Cunningham 2008).

The sedimentary dynamics of alluvial fans are influenced by numerous factors, such as the geology of the upstream lands, which are the sources of sediments, landslides, glaciers, and land use (Chen et al. 2010). Lucà (2012) and Santangelo et al. (2012) investigated the role of morphometry in sedimentation processes. Recent studies have examined the relationships between geology, vegetation, morphometry, and alluvial fan morphometry (Santangelo et al. 2012; Stokes and Gomes 2020; Lucà and Robustelli 2020). GIS techniques and principal component analysis (PCA) (Farhan et al. 2016), logistic regression (LR) (Stokes and Gomes 2020; Lucà and Robustelli 2020), and unsupervised self-organizing maps (SOMs) (Mokarram and Sathyamoorthy 2016) have been merged to investigate the types of alluvial fans and their distinctive morphometries. In recent studies, such as Basu et al. (2020), Ghosh and Gope (2021), and Ilanloo (2011) used fuzzy or ANN approaches to predict the morphometric characteristics of the watershed, and the benefits of both methods were not combined.

Therefore, there are watershed characteristics, such as alluvial fans, which are likely to be affected by tectonic and faulting activities where there is active subduction. In contrast, no study has discussed the use of precise methods such as PCA to identify the most important average morphometric features or how these parameters correlate with fault and erosion activities. Hence, in the study area, we combined PCA and artificial neural networks (ANNs) to predict tectonic and erosional activities based on morphometric characteristics.

The ANN is a predictive model that has been used in many geomorphological studies but has not yet been applied to the study and prediction of erosion based on alluvial fan morphometry. This study aims to

predict erosion from alluvial fan morphometry using the adaptive network-based fuzzy inference system (ANFIS) method. The alluvial fans in the vicinity of the Sabzevar and Sang-Sefid faults in northeastern Iran are the objects of study. This is among the few articles that have employed the ANN method to investigate and predict alluvial morphometries and their relationships to erosion in upstream watersheds (Lucà and Robustelli 2020). The PCA method was used to determine the most important morphometric parameters affecting the fault activity and soil erosion. This study is also innovative in that it strives to predict fault activity in the region based on the watershed's morphometric characteristics.

The remainder of this paper is organized as follows. section 2 explains the case study. In Section 3, the method of extracting alluvial fans is described. In addition, the formulation of the proposed method to select the important morphometric features and the predicted locations of faults based on morphometric features of the alluvial fan using PCA and ANFIS methods in Subsections 3.2 and 3.3. Section 4 describes the morphometric properties of the PCA and ANFIS methods. Finally, Section 5 concludes the paper.

Geological setting

The study area is located in the Central Desert watershed, located at 35°2'2" to 35°33'00" N and 57°38'24" to 59°06'24" E (Fig. 1). The study area covers 4,548 km^2. The Elevation in the area ranges from 861 to 2885 m. This region is located in the northern portion of central Iran and is limited to the north by the Alborz Mountains. To the east is the Lut block, and to the west is the Sanandaj-Sirjan zone. Coarse-grained and fine-grained sediments cover the surface of the plains. The faults in this region are active and are located in the Aladagh-Binalood Mountains (Rajabi et al. 2006).

These rocks are composed of ultramafic rocks along the Eurasian subcontinent. The Alpine-Himalayan fold is the last phase of this region. Its morphology is very young and the folds indicate that topography and geological structures have a direct relationship. These sediments folded in a similar way to the pressure regimes in this part of the world. The height of the region is mostly composed of mercenaries and Tirgans. It seems that plate movements have played a crucial role in the folding of sediments because of their

intensity along the southern front, as well as their asymmetry and steepness along the southwestern side. In addition, the movements caused the overlying faults along the landslide to split along the axis of the folds, drift with a slope to the north, and create faults along the foundation rock faults. In the Miocene, folding and drift movements began and monitoring of the strike-slip fault system at the end of the Pliocene led to structural sediment return in this region (Poursoltani et al. 2015). In this region, the primary sediments consist of conglomerate, sandstone, and a large amount of fine-grained sediments. A dark ophiolite boundary and a light gray limestone boundary are distinguishable in this sequence. Climatically, the average annual rainfall at the stations in the basin is 256.5 ± 35.11 mm. The average annual temperature is 13.99°C. The absolute maximum temperature of the period of study period was 48°C and the absolute minimum was -35°C.

Material and methods

Extracting the alluvial fans

Studies show that alluvial fans are formed by the accumulation of sediments from the mountain unit (Harvey et al. 2005) which are in the form of conical and their slope is more towards the mountain unit (about 35 degrees (Staley et al. 2006)) (Sanchez-Núñez et al. 2015) (Fig. 2 (a)). The top is the highest point on the fan and the closest location to the mountain unit. The cut channel, which is not always clear, is the alluvial channel that directs the sediment from the top to the downstream areas of the alluvial fan (Blair and McPherson 1994, 2009). Alluvial fans are formed by several transport mechanisms from mountain units. Alluvial fans have different shapes that are influenced by the bedrock, shape of the watershed, climate, and tectonics (Blair and McPherson 2009). The size of a fan is influenced by the size of the watershed; large alluvial fans are formed from large watersheds (Hooke 1968).

Alluvial fans were extracted from the study area using a semi-automatic method. A radial profile was prepared for each alluvial fan. Radial profiles are characterized by a conical shape with either a fixed slope or a downward and concave slope with a nearly flat slope downstream (Sánchez-Núñez et al. 2015). The morphometries of an alluvial fan can be a semi-conical surface. In the GIS algorithm, a conical surface is

created by joining a series of profiles radiating from the fan apex. The channels were mapped, the radial slopes were mapped, and the semi-conical surface was interpolated (Fig. 2(b)).

Radial profile analysis is mainly based on a fixed or variable minimum slope threshold that examines slope changes along each fan (slope threshold is defined by trial and error or training on a representative alluvial fan). The semi-conical surface of the alluvial fan was used to cut the radial profile. The apex is the location of the input of sediment input to the alluvial fan (Fig. 2(b)). In the next step, the topographic surface was placed on the radial profile to determine the shape of the alluvial fan. Profiles for all of the alluvial fans in the watershed were prepared from the DEM using a stepped process (Fig 3).

After extracting the alluvial fans, the morphometric parameters of both the fans and watersheds were determined (Table S1).

Asymmetric factor (Af), hypsometric integral index (Hi), and basin shape index (BS) were used to evaluate the effect of faults on watershed morphometry. The aim of this section is to investigate the effect of tectonic activity on the morphometric properties. Each of these indices is described below :

Symmetric Factor (*Af*)

The geometric network of rivers can be described both qualitatively and quantitatively. In areas where the drainage network develops in the presence of tectonic deformation, the drainage network often has a distinct geometric shape and pattern. The asymmetry factor has been linked to describe and understand the relationship between tectonic tilt in watersheds (Fig. S2). The Basin asymmetry was calculated (Eq. 1):

$$Af = 100(Ar - At) \quad (1)$$

where Ar is the area of the right part of the basin in the downstream direction relative to the main river, and At is the total area of the drainage basin. For the input network that is formed, and when the current is constant in the steady-state, Af = 47.7. Values above or below 47.7 indicate drainage basin tilt and tectonic activity (Hare and Gardner 1985; Keller and Pinter 2002).

Hypsometric integral index (*Hi*)

To determine the extent of geological activity, hypsometry was analyzed with Hi. The altimeter curve is the ratio of the total height of the basin to the total area of the basin (Strahler 1952; Keller and Pinter 2002). Although this index is not directly related to tectonics, it indirectly shows the distribution of the basin levels. This index was calculated (Eq. 2):

$$H_i = (h - H_{\min}) / (H_{\max} - H_{\min}) \quad (2)$$

where H_i is the hypsometric integral index, H_{max} is the maximum height, H_{min} is the minimum height, and h is the mean basin height. This index ranges from 0 to 5 for different regions. Higher values indicate a young topography, high elevation, and greater height than the average drainage network. Lower values indicate an equilibrium in the geomorphic processes and reduced tectonic activity.

Basin Shape Index (*BS*)

The shape of each region is directly related to internal and external influences on the watershed. In this regard, it can be concluded that forms are the result of these processes. High values of BS values indicate that tectonic activity occurred in the watershed. Basins with high tectonic activity were more elongated. They become more circular as tectonic activity diminishes during periods of erosion. The BS was calculated (Eq. 3):

$$BS = BI / BW \quad (3)$$

BS is the shape of the basin and indicates tectonic activity, BI is watershed length, and BW is watershed width.

PCA method

The most important morphometric parameters were determined by PCA. Thus, using the PCA method, the data (25 morphometric parameters) were reduced and the immaterial parameters were removed and the most important parameters were selected. PCA divides a similarity matrix into a set of axes or orthogonal

(vertical) components. Each axis represents a principal component (PC). The components were weighed and the variance was calculated for each axis, which is a specific value, an eigenvalue (Mellinger 1987; Pezhman et al. 2009). In PCA, the specific values of the similarity matrix are extracted in a stepwise downward trend; the components of the PCA indicate the amount of change they account for in the matrix. Therefore, the first PCA axes accounted for the highest percentage of definable changes. PCA is a variable reduction technique (Dillon and Goldstein 1984).

It is relevant to note that by linearly combining the initial variables $(X_1, X_2...X_n)$, new components will be created. As stated before, by changing the basis of the initial variables in the PCA method, these components prepare different aspects of the primary variables (Manly 1986). Equation 4 depicts the extraction of these components in detail.

$$Z_i = a_{ij}X_1 + a_{i2}X_2 + ... + a_{ip}X_p \quad (4)$$

where Z_i represents the desired component, a_{ij} is the coefficient of the primary variable, and X_i is the primary variable. The coefficients of the initial variables were obtained (Eq. 5):

$$| R - \lambda I | = 0 \quad (5)$$

where I is the unit matrix, R is the correlation matrix between the primary variables, and λ is the eigenvalue.

Adaptive Neural Fuzzy Method (ANFIS)

ANFIS was used in this study to predict the erosion rates. The ANFIS was introduced by Jang (1993). This method is based on the first-order Sugeno-fuzzy method. Because the fuzzy system is a very efficient modeling method, it has been widely used. Empirical knowledge is transformed into a mathematical map using linguistic rules. In systems where the knowledge of the expert is either unavailable or inaccurate, the neural network method can be used to create membership functions and rules for the system. For example, the two laws are defined by Eqs. Six and 7 (Bisht and Jangid 2011).

Rule 1: If $(x \in A_1)$ *and* $(x \in B_1(\text{ then })f_1 = p_1x + q_1y + r_1)$ (6)

Rule 2: If $(x \in A_2)$ and $(x \in B_2(, \text{then })f_2 = p_2x + q_2y + r_2)$ (7)

X and *y* are the inputs of the model, A_1 and B_1 are fuzzy sets, f_1 is the output of the model, and p_1, q_1, and r_1 are network design parameters. These rules had a general structure (Fig. S3(a)).

Layer 1: All the nodes are adaptive nodes. The output of Layer 1 is the degree of membership of the inputs, which are expressed in (Eqs. 8 and 9):

$$O_{1,i} = \mu A_i(x), \quad for\, i = 1,2 \tag{8}$$

$$O_{1,i} = \mu B_i(x), \quad for\, i = 3,4 \tag{9}$$

The membership functions is a Gaussian function (Eq. 10):

$$\mu A(x) = \frac{1}{1 + \left| \frac{x - c_i}{a_i} \right|^{2b_i}} \tag{10}$$

Layer 2: The output of this layer is the product of the input signals (Eq. 11).

$$O_{2,i} = w_i = \mu A_i(x)\mu B_i(y), \quad i = 1,2 \tag{11}$$

Layer 3: The output of this layer is normalized to that of the previous layer (Eq. 12):

$$O_{3,i} = \overline{w}_i = \frac{w_i}{w_1 + w_2}, \quad i = 1,2 \tag{12}$$

Layer 4: Normalized firing strength from layer 3 (Eq. 13):

$$O_{4,i} = \overline{w}_i f_i = \overline{w}_i (p_i x + q_i y + r_i) \tag{13}$$

Layer 5: The output of this layer is the output of the overall system (Eq. 14):

$$O_{5,i} = \sum_i \bar{w}_i f_i = \frac{\sum_i w_i f_i}{\sum_i w_i} \quad (14)$$

where x and y are the crisp inputs, and A_i and B_i are the language membership functions. P_i, q_i, and r_i are the sugar output parameters. The ANFIS also has a structure (Fig. S3 (b)) (Bisht and Jangid, 2011). it is operated in steps (Fig. S4).

All statistical calculations were performed using the (Statistical Package for Social Science (SPSS) v.22 and Matlab v. 17b.

Results and discussion

In this section, the results for predicting the faults based on the morphometric features of the alluvial fan are provided in subsections 3.1 3.4. To do this, in subsection 3.1, the morphometric properties of each alluvial fan are explained. In addition, in Subsection 3.2. important morphometric parameters for predicting soil erosion using the PCA method were selected. The ANFIS method to predict soil erosion is described in Section 3.3. in Section 3.4, the effect of faults on alluvial morphometry was investigated.

Morphometric properties

The alluvial fans of the study area were extracted using a semi-automatic method and a DEM (Fig. 4). There were 54 alluvial fans in the study basin, most of which were affected by the Sabzevar faults and the Sang- Sefid fault. The morphometric properties of the 54 alluvial fans were determined using GIS (Table 1).

The mean values for each of the morphometric features of the alluvial fan and its upstream watershed were determined (Table 1). The maximum and minimum A_f are 38.63 and 0.75 km^2, respectively. The maximum L_f is 9.59 and the minimum L_f is 1.43. The minimum alluvial fan elevation was 985 m and the maximum alluvial fan elevation was 1,392 m. The maximum value of $R_{rf\text{-}L}$ was 1,724.93. The maximum

slope was 49.5°. The maximum R_f is 9. The maximum angle of the alluvial fan was 86 ° and the lowest was 31° °. The lowest and highest *BS* values are 0.82 and 3.9, respectively. The highest *value of Cirb* was 6.91.

The maximum V_f is 11.6. The morphometric characteristics of the recharged watershed of each alluvial fan were also determined. The maximum and minimum fan areas in the basin is 62.52 and 0.46 km^2. The maximum and minimum elevations were 2,077 and 1,022 m, respectively. The maximum and minimum L_b values are 11.77 0.63. The maximum and minimum slopes were 86° ° and 30°°, respectively. The maximum and minimum values of *Mel* are 7.9 3.83.

The relationship between A_f, V_f, and A_b was examined (Fig. 5). There was a significant positive relationship between A_f and V_f with A_b (R^2 = 0.91 for A_b and A_f, and R^2 = 0.82 and).

Selecting the important morphometric parameters using PCA

Considering the concentrations of erosion constituents at various monitoring stations, PCA was performed (Fig. 6). The first (40.72%) and second (18.16%) PCs together explained approximately 58.88 % of the variance at the stations. The average distribution of weights allocated to the first, second, and third components was also determined for the 54 alluvial fans (Fig. S5).

The distribution of the weights of the parameters in each of the first, second and third principal components was graphed (Fig. S5). Parameters A_f, P_f, L_f, R_f, V_f, P_b, A_b, *LC*, L_b, *Dd*, and formation material had the greatest weights (Table 2). Those that were farthest from the components' lines were the parameters with the greatest influence on erosion.

The results of Kaiser–Meyer–Olkin (KMO) and Bartlett's sphericity tests showed that the significance level was < 0.01, indicating that there were significant relationships among variables in this analysis (Kaiser, 1974. Analysis of variance showed that the parameters that have significant relationships with erosion were H_{max}_f, *α, BS, Mel, CC, and Dd.* $R_f f$, $\beta_{min\text{-}f}$, R_f, *CC, LC,* $R_r b$, *Dd*, and formation material were significantly related to lithology (Table 3). The results of Srivastava and Bhattacharya (1998) and Farhan et al. (2017) showed that PCA is suitable for selecting the most morphometric features in a watershed.

295

296 **Results of ANFIS**

297 Grid partitioning, subtractive, and FCM models were used to predict soil erosion using the ANFIS.
298 Hybrid and backpropagation modes were used for each model (run in MATLAB). The results showed that
299 modeling soil erosion in the study area using the subtractive method had the lowest error (Fig. S6 and Table
300 4). Two radii of 0.01 and 0.03, were used. The hybrid method with radii of 0.01 and 0.03 had R^2= 0.99,
301 MSE=0, and RMSE= 0.03, and high accuracy. This method requires four rules (Fig. S7).

302 The relationships between the parameters A_f, A_b, P_f, R_f, L_f, and soil erosion in the three dimensions are
303 shown (Fig. S8). The results of Gholami et al. (2018) showed that the ANFIS method is an accurate method
304 for predicting parameters in a watershed.

305 In general, several features are found in a fuzzy neural network, such as learning power, as well
306 as costing, classifying, writing, and compiling. Another advantage is that it allows the extraction
307 of fuzzy rules from a variety of information and calculates the basic rules proportionally. Fuzzy
308 neural networks have been proven to have the ability to model multiple processes in recent studies
309 to predict the erosion rate (Nguyen et al. 2020). The artificial neural network (ANN) model
310 performs better when there is sufficient information and data. Observational data are used to train
311 the network, so the system's performance is reduced when there is a lack of data. in the fuzzy
312 inference system, the input and output variables in this model are described linguistically. Because
313 there is no formal method for doing this, the fuzzy system uses innovative approaches when the
314 information is incomplete and contradictory. This is usually time-consuming and error-prone.
315 Nauck and Kruse (1999) used both fuzzy rule generation capability and network training capability
316 in the ANN model, thus overcoming the shortcomings of each and creating the ANFIS method.
317 Some studies have shown that the ANFIS method is extremely accurate in some natural sciences,
318 such as groundwater prediction (Elzain et al. 2021; Seifi et al. 2020), soil (Mehdizadeh et al. 2020),

predicting erosion (Islam et al. 201; Kaboodvandpour et al. 2015), and water quality (Fu et al. 2020), and can provide better results than ANN and fuzzy models.

Results of A_f, H_i, and BS

The effects of faults on alluvial morphometry using A_f, H_i, and BS were investigated. The results for A_f indicated that watersheds (sub-basins) 11, 37, 31, 29, 36, 34, 39, 26, 44, 21, 50 ,30, 28, 25, 27, 18, 49, 5, 24, 53, and 12, with values of A_f <35 or A_f> 65, are in class 1. Watersheds 35, 23, 47, 32, 41, 13, 48, 6, 3, 17, 20, 14, and 9, with values 57 <A_f < 65 or 35 <A_f <43, are in class 2. And watersheds 45, 33, 38, 46, 19, 10, 16, 40, 51, 2, 54, 4, 52, 42, 22, 15, 43, 1, 7, and 8, with 43 <A_f <57, are in class 3. According to the classification by Hamdoni et al. (2008), the sub-basins in class 1 have high tectonic activity (Table 5).

Hi was calculated for the sub-basins using the GIS software. Watersheds 21-34 and 43-54 have the highest Hi (> 0.5), indicating that they are areas of high tectonic activity. Watersheds 1-20 and 35-41 had the lowest Hi (< 0.4), indicating less tectonic activity in these sub-basins (Fig. 7).

The BS values indicate that most watersheds have a coefficient higher than 1, indicating elongated basins and high tectonic activity in these areas (Fig. 8).

The tectonic state of a region can be determined using morphometric features. Bahrami (2013) also concluded that there is a relationship between the morphometric properties of alluvial fans located in Zagros, Iran and the tectonic state. In this study, morphometric features affecting soil erosion were identified using PCA. The parameters A_f, P_f, L_f, R_f, V_f, P_b, A_b, LC, L_b, Dd, and formation material are the 25 most useful parameters for predicting erosion (Sharma et al. 2015). As a result, there was a strong correlation between tectonic activity and the morphometric characteristics of alluvial fans in the study area. Therefore, the morphometric characteristics of alluvial fans can be used to determine tectonic activity in an area (Bahrami 2013; Hashemi et al. 2018; Yamani et al. 2012).

Conclusion

The results show that A_f, P_f, L_f, R_f, V_f, P_b, A_b, LC, L_b, Dd, and formation material had the greatest influence on erosion rates in the study area. PCA was used to identify the most important parameters influencing erosion. Using ANFIS, the soil erosion in the study area was predicted using these parameters. The effects of two large Sabzevar faults and the Sang-e-Sefid fault on the morphometric characteristics of alluvial fans and their watersheds were also investigated. The results showed that tectonic activity was the main factor in the formation, development, and evolution of alluvial fans in the study area. The Sabzevar and Sang-e-Sefid faults have been more influential on morphometry than other tectonic factors. The results show that faults are active in the study area and affect the morphometry of the watershed. One of the most important outcomes of this study is the confirmation of the ability to identify and predict the tectonic activities of the watershed quantitatively.

Data availability

The data will be available through the corresponding author

Author contributions

Conceptualization by M.M. and H.R.P.; formal analysis by M.M., H.R.P.; initial methodology and investigation by M.M., H.R.P.J.P.T.; project administration by J.P.T., supervision by H.R.P., and M.M.; validation by J.P.T., H.R.P. and M.M.; visualization and software by M.M.; writing—original draft by and M.M. and H.R.P.; writing—by J.P.T.

Competing interests

The authors declare that they have no conflict of interest.

Special issue statement

Not.

Acknowledgements

The authors would like to thank Shiraz University for providing financial support (grant number: 289432-209) for this study.

Financial support

This research is supported by Shiraz University.

References

Bahrami S (2013) Tectonic controls on the morphometry of alluvial fans around Danehkhoshk anticline, Zagros, Iran. Geomorphology (180: 217-230.

Beaty CB (1963) Origin of Alluvial Fans, White Mountains, California and Nevada, Ann. Am. Assoc. Geogr Vol. 53: PP. 516-535.

Benito G (2013) Hazardous processes: flooding. In: Shroder, J. (Ed.), Treatise on geomorphology. Geomorphology of Human Disturbances, Climate Change, and, Natural Hazards. Academic Press, San Diego, CA 243–261.

Bisht DCS, Jangid A (2011) Discharge modelling using adaptive neuro-fuzzy inference system. Int. J. Adv. Sci. Technol, 31 (2011), 99–114

Blair T, McPherson J (1994) Alluvial fan processes and forms. In: Parsons, A.J, Abrahams, A.D. (Eds.), Geomorphology of Desert Environments. Chapman & Hall, London, 354–402.

Blair TC, McPherson JG (2009) Processes and forms of alluvial fans. In: Parsons, A.J, Abrahams, A.D. (Eds.), Geomorphology of Desert Environments, second ed. Springer, Berlin, 413–467.

Bull WB (2007 Tectonic Geomorphology of Mountains , A New Approach to Paleosiesmology, Blackwell, 316.

Chen CH, Wang CH, Hsu YJ, Yu SB, Kuo LC (2010) Correlation between groundwater level and altitude variations in land subsidence area of the Choshuichi Alluvial Fan, Taiwan. Eng. Geo 115(2): 122-131

Dillon WR, Goldstein R (1984) Multivariate Analysis Methods and Application. John Wiley and Sons. 453 pp

Eisank C, Smith M, Hillier J (2014) Assessment of multiresolution segmentation for delimiting drumlins in digital elevation models. Geomorphology, 214: 452–464.

Farhan Y, Anbar A, Al-Shaikh N, Mousa R (2016) Prioritization of semi-arid agricultural watershed using morphometric and principal component analysis, remote sensing, and GIS techniques, the Zerqa River Watershed, Northern Jordan Agric Sci 8(1): 113-148

Farhan Y, Anbar A, Al-Shaikh N, Mousa R (2016) Prioritization of semi-arid agricultural watershed using morphometric and principal component analysis, remote sensing, and GIS techniques, the Zerqa River Watershed, Northern Jordan. Agric. Sci. 8(1): 113-148

Fleming C, Marsh SH, Giles JRA (2010) Introducing elevation models for geoscience. In: Fleming, C, Marsh, S.H, Giles, J.R.A. (Eds.), Elevation Models for Geoscience. Geological Society, London, Special Publication 345: 1–4.

Foster NH, Beaumont EA (1992) Photogeology and photogeomorphology. American Association of Petroleum Geologists, Tulsa, OK, USA.

Gholami A, Bonakdari H, Ebtehaj I, Gharabaghi B, Khodashenas SR, Talesh SHA, Jamali A (2018) A methodological approach of predicting threshold channel bank profile by multi-objective evolutionary optimization of ANFIS. Eng Geo 239: 298-309

Hamdouni RE, Irigaray C, Fernandez T, Chacon J, Keller EA (2008) Assessment of relative active tectonic, south west border of the sierra novada. (Southern Spain). Geomorphology 96: 150- 173.

Hare PW, Gardner TW (1985) Geomorphic indicators of vertical neotectonism along converging plate margins, Nicoya Peninsula, Costa Rica. In: Morisawa M, Hack JT (Eds.) Tectonic Geomorphology. Proceedings of the 15th Annual Binghamton Geomorphology Symposium. Allen and Unwin, Boston,123-134.

Harvey A, Mather AE, Stokes M (2005) Alluvial fans: geomorphology, sedimentology, dynamics-introduction, a review of alluvial fan research. In: Harvey, A, Mather, A.E, Stokes, M.

(Eds.), Alluvial fans: geomorphology, sedimentology, dynamics. Geological Society Special Publication 251, London, 1–8.

Harvey AM, Wells SG (1987) Response of Quaternary fluvial systems to differential epeirogenic uplift: Aguas and Feos river systems, southeast Spain. Geo 15(8): 689-693

Harvey AM, Wigand PE, Wells SG (1999) Response of alluvial fan systems to the late Pleistocene to Holocene climatic transition: contrasts between the margins of pluvial Lakes Lahontan and Mojave, Nevada and California, USA. Catena, 36(4): 255-281

Hooke RL (1968) Model geology: prototype and laboratory streams: discussion. Geol. Soc. Am. Bull. 79: 391–394

Jang JS (1993) ANFIS: adaptive-network-based fuzzy inference system. IEEE transactions on systems, man, and cybernetics 23(3): 665-685

Kaiser H (1974) An index of factorial simplicity. Psychometrika, 39: 31-6.

Keller EA, Pinter N (2002) Active Tectonics: Earthquakes, Uplift, and Landscape (2nd Ed.). Prentice Hall, New Jersey

Khan MA, Haneef M, Khan AS, Tahirkheli T (2013) Debris-flow hazards on tributary junction fans, Chitral, Hindu Kush Range, northern Pakistan. J Asian Earth Sci 62: 720–733.

Lagmay AMF, Eco RN, Alconis J, Salvio B (2013) What hit Barangay Andap, New Bataan, Compostela Valley (initial assessment). Project NOAH Open-File Report, Manila, Philippines.

Lancaster J, Spittler T, Short W (2012) Using digital geologic maps to assess alluvial-fan flood hazards. In: Soller, D.R. (Ed.), Digital Mapping Techniques Workshop Proceedings. U.S. Geological Survey Open-File Report 1171, Washington, USA, 53–64.

Langer WH, Drew LJ, Sachs JS (2004) Aggregate and the environment: American Geological Institute Environmental Awareness, Series 8: 64.

447 Lucà F (2012) Valutazione di pericolosità geomorfologiche indotte da fenomeni naturali
448 tramite l'applicazione di modelli statistico– matematici. (PhD dissertation) University of
449 Calabria Rende (CS) Italy 204 pp.
450 Lucà F, Robustelli G (2020) Comparison of logistic regression and neural network models in
451 assessing geomorphic control on alluvial fan depositional processes (Calabria, southern Italy).
452 Environ Earth Sci 79(1): 1-18
453 Manly BF (1986) Multivariate Statistical Methods: A Primer. London, UK: Chapman and
454 Hall.
455 Mellinger M (1987) Multivariate data analysis: its methods. Chemometrics and Intelligent
456 Laboratory Systems 2: 29-36.
457 Mokarram M, Sathyamoorthy D (2016) Clustering of landforms using self-organizing maps
458 (SOM) in the west of Fars province. In IOP Conf. Series: Earth Environ Sci 37: 012009.
459 Parsons T (2009) Lasting earthquake legacy. Nature, 462(7269): 42-43
460 Pezhman HA, Nabi Bidhendi GH, Karbasi AR, Mehrdadi N, Bidhendi ME (2009) Evaluation
461 of spatial and seasonal variations in surface water quality using multivariate statistical
462 techniques, Int J Environ Sci Technol 6: 467-476
463 Radebaugh J, Lorenz RD, Farr TG, Kirk RL, Lunine JI, Ventra, D Le Gall A, Lopes RMC,
464 Barnes JW, Hayes A, Stofan ER, Wall SD, Wood C (2013) Alluvial fans on Titan reveal
465 materials, processes and regional conditions. 44th Lunar and Planetary Science Conference, The
466 Woodlands, Texas, USA, 2641.
467 Roberts N, Cunningham D (2008) Automated alluvial fan discrimination, Quaternary fault
468 identification, and the distribution of tectonically reactivated crust in the Gobi Altai region,
469 southern Mongolia. Int. J. Remote Sens 29(23): 6957-6969

Sánchez-Núñez JM, Macías JL, Saucedo R, Zamorano JJ, Novelo D, Mendoza ME, Torres-Hernández JR (2015) Geomorphology, internal structure and evolution of alluvial fans at Motozintla, Chiapas, Mexico. Geomorphology 230 (1–12.

Santangelo N, Daunis-i Estadella J, Di Crescenzo G, Di Donato V, Faillace PI, Martín-Fernández JA, Romano P, Santo A, Scorpio V (2012) Topographic predictors of susceptibility to alluvial fan fooding Southern Apennines. Earth Surf Process. 37:803–817

Sharma SK, Gajbhiye S, Tignath S (2015) Application of principal component analysis in grouping geomorphic parameters of a watershed for hydrological modeling. Appl Water Sci 5(1): 89-96

Srivastava HN, Bhattacharya SN (1998) Application of principal component analysis to some earthquake related data in the Koyna region, India Engin Geo 50(1-2): 141-151

Staley DM, Wasklewicz TA, Blaszczynki JS (2006) Surficial patterns of debris flow deposition on alluvial fans in Death Valley, CA using airborne laser swath mapping data. Geomorphology 74: 152–163

Stokes M, Gomes A (2020) Alluvial fans on volcanic islands: A morphometric perspective (São Vicente, Cape Verde). Geomorphology 368: 107356

Strahler AN (1952) Hypsometric (area-altitude) analysis of erosional topography. Geol Soc Am Bull 63(11): 1117-1142

Sancho C, Peña, JL, Rivelli F, Rhodes E, Muñoz A (2008) Geomorphological evolution of the Tilcara alluvial fan (Jujuy Province, NW Argentina): Tectonic implications and palaeoenvironmental considerations. J S Am Earth Sci 26(1), 68-77

Stokes M, Mather AE (2000) Response of Plio-Pleistocene alluvial systems to tectonically induced base-level changes, Vera Basin, SE Spain. J Geol Soc 157(2), 303-316

493 Nauck, D, Kruse, R, (1999), Obtaining Interpretable fuzzy Classification Rules from Medical
494 Data, Artif Intell Med 16 (2), PP (149–169

495 Seifi A, Ehteram M, Singh VP, Mosavi A (2020) Modeling and uncertainty analysis of
496 groundwater level using six evolutionary optimization algorithms hybridized with ANFIS, SVM,
497 and ANN. Sustainability 12(10), 4023

498 Elzain HE, Chung SY, Park KH, Senapathi V, Sekar S, Sabarathinam C, Hassan M (2021)
499 ANFIS-MOA models for the assessment of groundwater contamination vulnerability in a nitrate
500 contaminated area. J Environ Manage 286, 112162

501 Fu Z, Cheng J, Yang M, Batista J, Jiang Y (2020) Wastewater discharge quality prediction using
502 stratified sampling and wavelet de-noising ANFIS model. Comput Electr Eng 85, 106701

503 Mehdizadeh S, Ahmadi F, Kozekalani Sales A (2020) Modelling daily soil temperature at
504 different depths via the classical and hybrid models. Meteorol. Appl 27(4), 1941
505 Nguyen KA, Chen W, Lin BS, Seeboonruang U (2020). Using Machine Learning-Based
506 Algorithms to Analyze Erosion Rates of a Watershed in Northern Taiwan. Sustainability 12(5),
507 2022

508 Kaboodvandpour S, Amanollahi J, Qhavami S, Mohammadi B (2015) Assessing the accuracy of
509 multiple regressions, ANFIS, and ANN models in predicting dust storm occurrences in Sanandaj,
510 Iran. Nat Hazards 78(2), 879-893

511 Islam MR, Jaafar WZW, Hin LS, Osman N, Hossain A, Mohd NS (2018) Development of an
512 intelligent system based on ANFIS model for predicting soil erosion. Environ Earth Sci 77(5), 1-
513 15

514 Poursoltani MR, Jamali M, Nasiri Y (2015) Lithofacies, Petrofacies and depositional
515 environment of Jurassic deposits in Binalood Zone in the Bazeh hoz section, South of
516 Mashhad. Applied Sedimentology 3(6), 82-102

517 Ilanloo M (2011) A comparative study of fuzzy logic approach for landslide susceptibility
518 mapping using GIS: An experience of Karaj dam basin in Iran. Procedia Soc Behav Sci 19, 668-
519 676

520 Ghosh M, Gope D (2021) Hydro-morphometric characterization and prioritization of sub-
521 watersheds for land and water resource management using fuzzy analytical hierarchical process
522 (FAHP): a case study of upper Rihand watershed of Chhattisgarh State, India. Appl Water Sci
523 11(2), 1-20

524 Basu T, Das A, Pal, S (2020) Application of geographically weighted principal component
525 analysis and fuzzy approach for unsupervised landslide susceptibility mapping on Gish River
526 Basin, India. Geocarto Int 1-24

527 Hashemi F, Derakhshani R, Bafti SS, Raoof A (2018) Morphometric dataset of the alluvial fans
528 at the southern part of Nayband fault, Iran. Data brief 21, 1756-1763

529 Bahrami S (2013) Tectonic controls on the morphometry of alluvial fans around Danehkhoshk
530 anticline, Zagros, Iran. Geomorphology 180, 217-230

531 Yamani M, Maghsoudi M, Ghassemi MR, Mohammadnejad V (2012) Morphologic and
532 Morphometric Evidence for Active Tectonic Effects on Alluvial Fans in North Damghan. Phys
533 Geog Res 44(2), 1-18

534

535 **Table 1.** Morphometric features of alluvial fans in the study area

Parameters	Minimum	Maximum	Average	STDVI
A_f	0.75	38.63	6.62	7.68
P_f	3.57	26.84	9.88	5.6
L_f	1.43	9.59	3.85	2.2
H_{min}_f	985	10990	1292.19	1348.05
H_{max}_f	1036	1392	1217.39	100.91
ΔH_f	1010.5	6054.5	1254.79	672.1
R_f _L	120.8	1724.93	418.59	263.81
β_f	5.35	49.5	29.73	8.28
R_f	0.49	9	2.19	1.42
Erosion	3	7	6.07	1.03
α	31	86	62.31	12.54
BS	0.82	3.9	1.92	0.62
Cirb	0.64	6.91	2.44	1.66
V_f	0.11	11.6	1.89	2.41
P_b	2.74	33.66	11.93	7.31
A_b	0.46	62.52	11.75	13.91
H_{min}_b	1022	1411	1216.31	112.65
H_{max}_b	1049	2077	1542.59	307.47
$\Delta H_{b/L}$	4	813	326.28	232.46
L_c	0.63	11.77	3.68	2.7
L_b	1.03	13.56	4.64	3.02
ΔHb	0.88	247.02	81.03	54.37
β_b	30	86	72.37	12.08
D_d	141.5	1135	759.1	257.82
Mel	3.83	7.9	13.79	7.82

536

537 **Table 2.** Special vector of each parameters using the PCA method

Code	Parameters	Component					
		1	2	3	4	5	6
A	A_f	.928	-.048	.030	-.116	.169	.044
B	P_f	.969	-.041	.089	-.101	.053	.064
C	L_f	.941	.001	.225	-.075	-.040	.047
D	H_{min}_f	-.090	-.210	.242	.794	.261	.315
E	H_{max}_f	.143	.726	.222	.271	-.108	-.461
F	R_f	-.629	-.038	.105	.656	.281	.105
G	$\beta_{min\text{-}f}$	-.305	.690	-.193	.060	-.131	-.045
H	$\beta_{max\text{-}f}$	.094	.075	-.095	.172	-.492	-.129
I	R_f	.838	-.078	-.234	-.129	.355	.092
J	α	-.232	.186	.594	-.293	.414	-.237
K	BS	-.029	-.061	.737	-.089	-.404	.125
L	V_f	.878	.024	.099	-.168	.314	.007
M	P_b	.965	-.044	.040	.128	-.046	-.041
N	A_b	.935	-.048	.081	.030	.004	-.054
O	H_{min}_b	.172	.812	.272	.219	.076	-.375
P	H_{max}_b	.537	.813	.020	.059	.062	.053
Q	*Mel*	-.461	-.006	.545	-.372	-.003	.244
R	CC	.012	-.056	-.699	-.141	.113	-.233
S	*LC*	.930	-.096	.125	.113	-.023	-.034
T	L_b	.935	-.077	.138	.150	-.059	-.016
U	R_rb	-.166	.823	-.262	-.120	.036	.284
V	$\beta_{min\text{-}b}$	.150	.781	-.113	-.005	-.166	.417
W	$\beta_{max\text{-}b}$	.249	.856	-.035	-.088	.096	.252
X	Dd	.815	-.147	-.248	.284	-.059	.013
Y	Geology unit	.767	-.230	-.030	.056	-.411	.099

538

539 **Table 3**. Analysis of variance of parameter values
540

		Erosion					Lithology				
Code	**Parameters**	**Sum of Squares**	**df**	**Mean Square**	**F**	**Sig.**	**Sum of Squares**	**df**	**Mean Square**	**F**	**Sig.**
A	A_f	110.666	3	36.889	.612	.610	275.688	5	55.138	.930	.470
B	P_f	86.282	3	28.761	.914	.441	149.084	5	29.817	.948	.459
C	L_f	19.884	3	6.628	1.406	.252	20.742	5	4.148	.848	.523
D	H_{min}_f	1898599.934	3	632866.645	.335	.800	5.329	1	5.329	1.089	.302
E	H_{max}_f	113876.637	3	37958.879	4.458	.008	6.919	1	6.919	1.414	.240
F	$R_f f$	220379.409	3	73459.803	1.059	.375	22166497.023	5	4433299.405	2.870	.024
G	$\beta_{min\text{-}f}$	226.071	3	75.357	.920	.438	219793.633	5	43958.727	6.597	.000
H	$\beta_{max\text{-}f}$	120.235	3	40.078	.217	.884	466141.586	5	93228.317	1.389	.245
I	R_f	3.185	3	1.062	.509	.678	2616.331	5	523.266	14.741	.000
J	α	1849.880	3	616.627	4.757	.005	808.241	5	161.648	.909	.483
K	BS	4.039	3	1.346	4.086	.011	9.926	5	1.985	.976	.442
L	V_f	19.254	3	6.418	1.111	.353	1378.765	5	275.753	1.904	.111
M	P_b	213.538	3	71.179	1.358	.266	1.270	5	.254	.634	.675
N	A_b	621.650	3	207.217	1.076	.368	31.870	5	6.374	1.108	.369
O	H_{min}_b	72939.452	3	24313.151	2.027	.122	5.216	1	5.216	.906	.346
P	H_{max}_b	340177.989	3	113392.663	1.214	.314	150.057	5	30.011	.536	.748
Q	*Mel*	83709.498	3	27903.166	3.289	.028	771.637	5	154.327	.782	.568
R	CC	.094	3	.031	2.370	.082	256793.148	5	51358.630	5.930	.000
S	*LC*	17.433	3	5.811	.785	.508	1140675.212	5	228135.042	2.830	.026
T	L_b	33.181	3	11.060	1.228	.309	46815.179	5	9363.036	.975	.443
U	R_b	16768.019	3	5589.340	1.997	.126	.162	5	.032	2.604	.037
V	$\beta_{min\text{-}b}$	293.478	3	97.826	.594	.622	25.736	5	5.147	.683	.638
W	$\beta_{max\text{-}b}$	498.113	3	166.038	.606	.614	35.014	5	7.003	.749	.591
X	Dd	487089.803	3	162363.268	2.674	.057	63091.729	5	12618.346	6.471	.000

541
542 **Table 4.** Results of three models for predicting soil erosion

Methods	**Different modes**	**Model**	**Training error**			**Test error rate (test)**		
			MSE	**RMSE**	**R**	**MSE**	**RMSE**	**R**
Grid	5	Back propagation	0.003	0.03	0.66	0.03	0.03	0.66
		Hybrid	0.002	0.02	0.79	0.03	0.03	0.79
	10	Back propagation	0.003	0.04	0.67	0.04	0.05	0.68
		Hybrid	0.002	0.04	0.78	0.03	0.03	0.78
Subtractive	0.3	Back propagation	0.001	0.04	0.91	0.003	0.04	0.92
		Hybrid	0	0.0304	0.99	0	0.0303	0.99
	0.01	Back propagation	0.001	0.04	0.9	0.004	0.04	0.89
		Hybrid	0	0.0305	0.99	0	0.0303	0.99
FCM	5	Back propagation	0.02	0.04	0.78	0.03	0.03	0.78
		Hybrid	0.03	0.04	0.81	0.03	0.02	0.81
	10	Back propagation	0.02	0.04	0.82	0.03	0.02	0.82
		Hybrid	0.04	0.03	0.88	0.04	0.03	0.87

543
544 **Table 5.** The slope coefficient of the studied basins

Code	**A_t**	**A_r**	**A_f**	**Code**	**A_t**	**A_r**	**A_f**
1	35.78	20	55.9	28	1.91	0.59	30.92
2	15.96	7.8	48.86	29	2.87	0.62	21.62
3	5.47	2.3	42.08	30	1.7	0.51	29.98
4	0.99	0.5	50.65	31	0.49	0.1	20.58
5	2.24	0.8	35.76	32	1.11	0.44	39.53
6	3.11	1.3	41.77	33	0.47	0.21	45.02
7	7.84	4.4	56.11	34	0.46	0.11	23.94
8	3.74	2.1	56.19	35	26.69	10	37.47
9	5.37	3.37	62.75	36	15.48	3.6	23.26
10	6.67	3.16	47.36	37	38.76	7	18.06
11	33.84	2.2	6.5	38	33.26	15	45.09
12	32.06	24.8	77.35	39	41.24	10	24.25

13	17.35	7	40.35	40	49.95	24	48.05
14	12.56	7.4	58.91	41	62.52	25	39.99
15	6.75	3.7	54.85	42	17.82	9.1	51.07
16	6.71	3.2	47.72	43	5.24	2.9	55.38
17	8.38	3.6	42.98	44	10.63	3	28.22
18	4.62	1.5	32.45	45	6.47	2.9	44.8
19	3.68	1.7	46.21	46	5.5	2.5	45.49
20	3.47	1.5	43.17	47	12.66	5	39.5
21	1.94	0.55	28.35	48	6.3	2.6	41.24
22	1.33	0.68	51.16	49	6.6	2.3	34.86
23	1.24	0.47	38.03	50	11.58	3.3	28.5
24	0.92	0.33	36	51	14.49	7	48.31
25	3.79	1.2	31.68	52	11.24	5.7	50.71
26	3.72	1	26.9	53	10.21	7	68.56
27	1.03	0.33	32.01	54	8.51	4.2	49.35

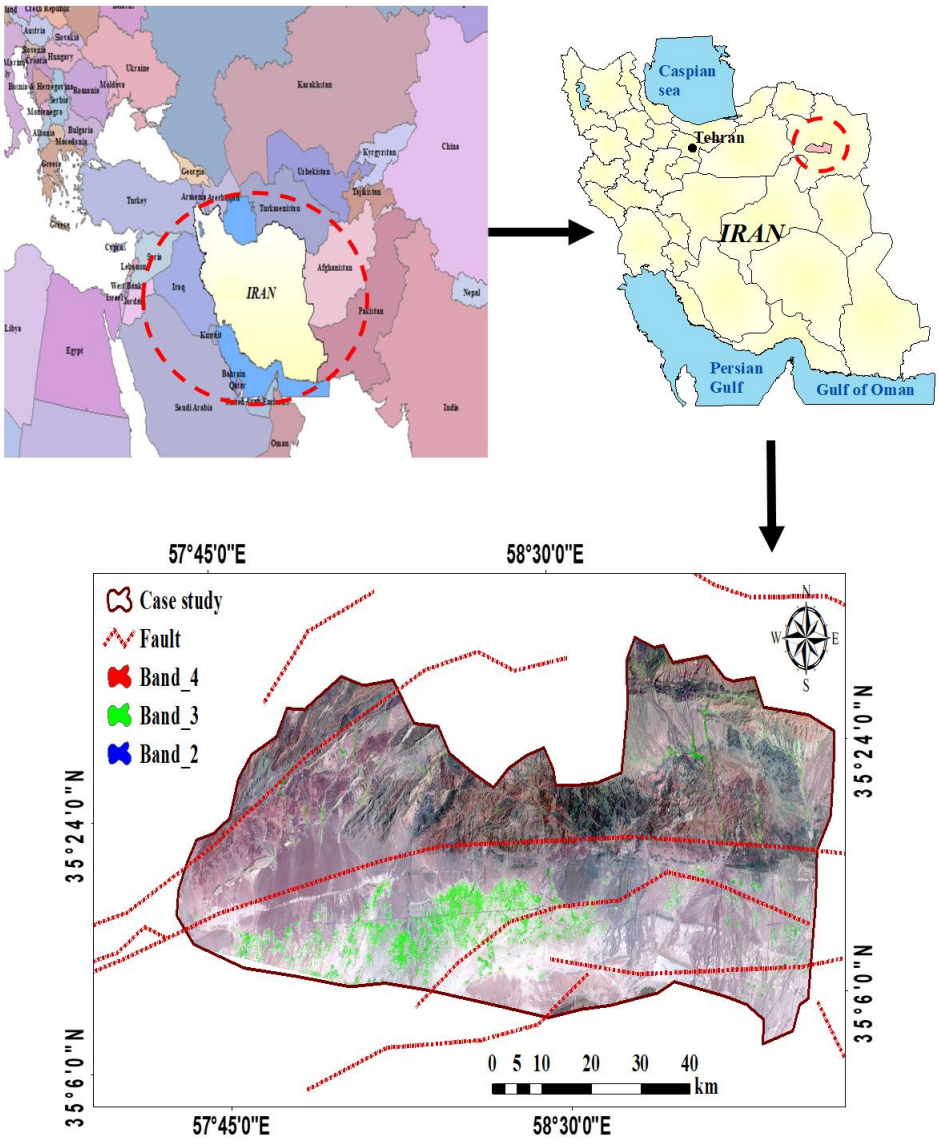

Fig. 1. Location of the study area

Landsat 8 satellite imagery (Enhanced Thematic Mapper Plus (ETM+) sensor), band combination 432

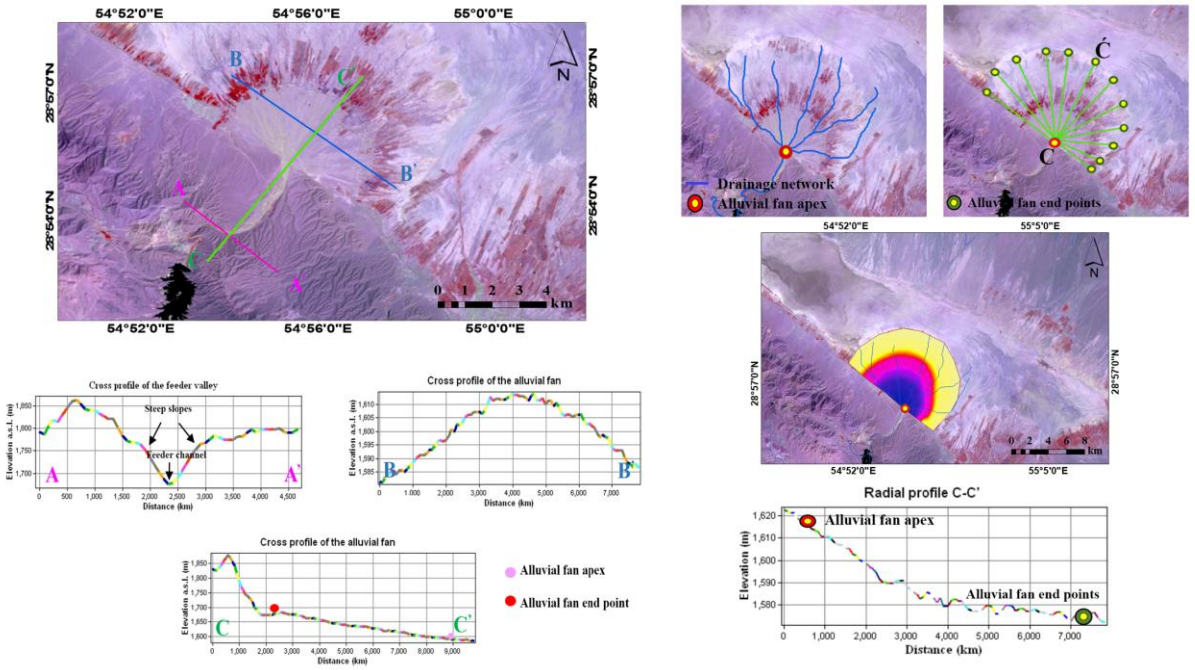

Fig. 2. (a): Morphological status of a large alluvial fan (a) the alluvial fan from satellite images (b) topographic characteristics of AA', BB', CC' profiles, (b): The steps to extract the alluvial fan with the GIS algorithm: (A) hydrological analysis using drainage network; (B) the radial profiling and determination of alluvial fan endpoints; and (C) interpolation of the semi-conical surface.

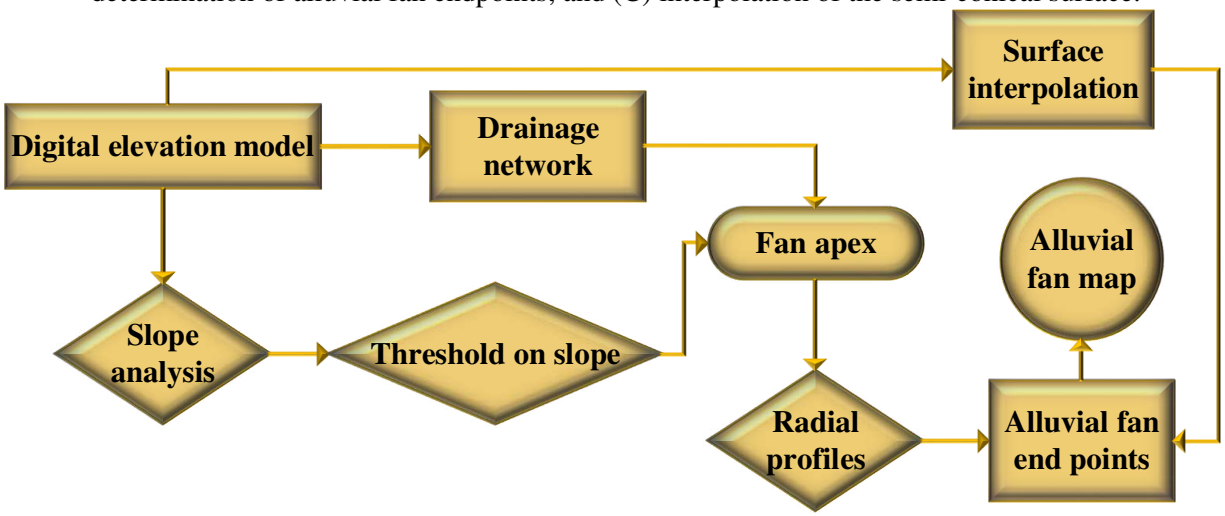

Fig. 3. Flowchart of alluvial fan extraction from DEM.

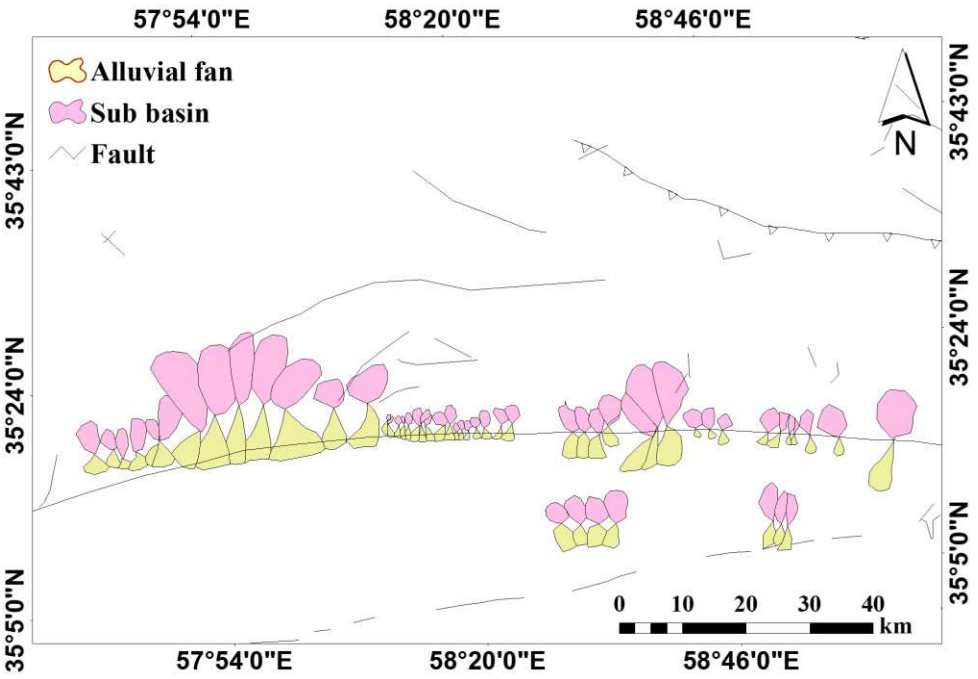

Fig. 4. Position of alluvial fans in the study area

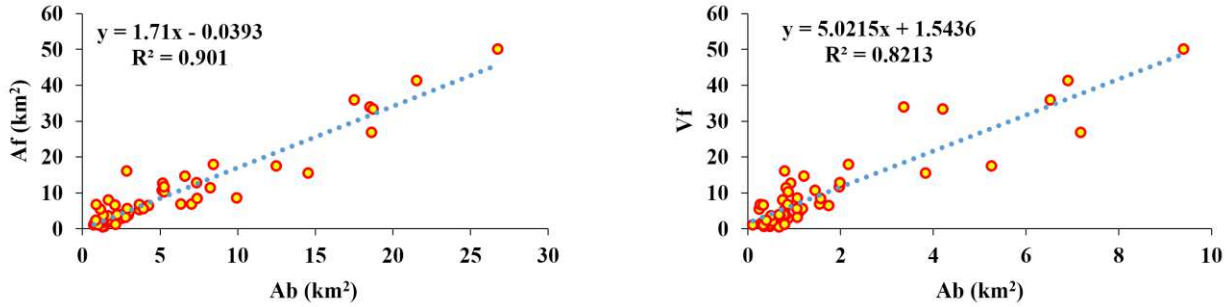

Fig. 5. Relationship between A_f, A_b, V_f

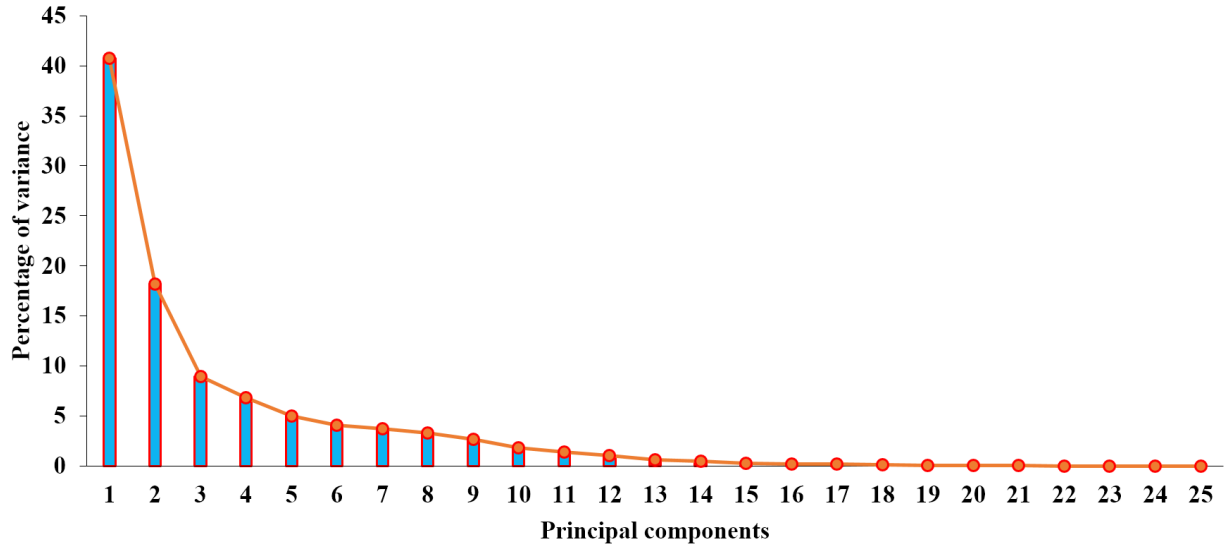

Fig. 6. Percentage of variance expressed by the first 14 principal components for erosion

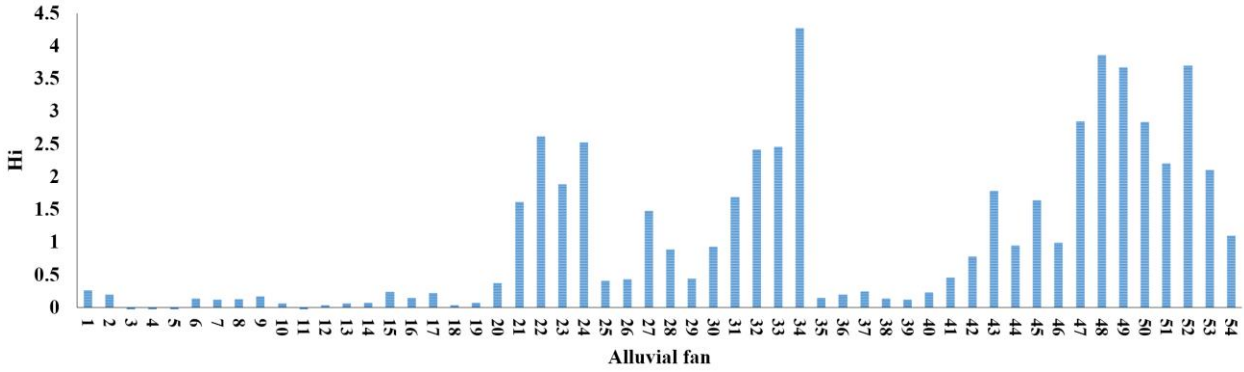

Fig. 7. Altimetry integral values for the sub-basins

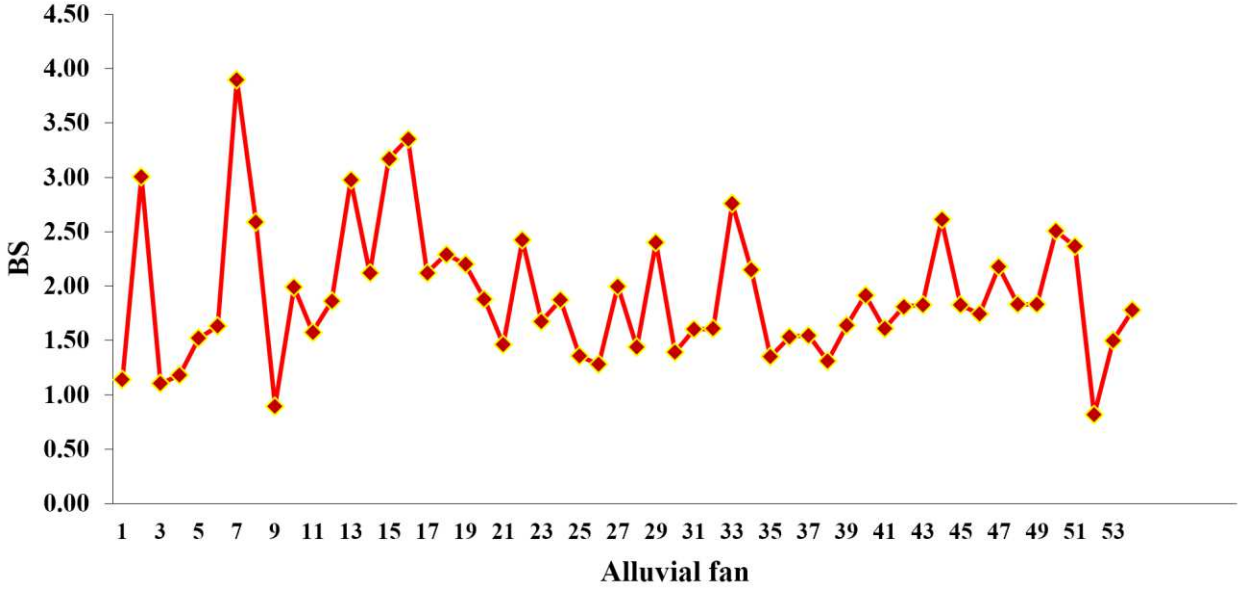

Fig. 8. BS values for each of the sub-basins

Supplementary Files

This is a list of supplementary files associated with this preprint. Click to download.

- Supplementary2.docx